# Crosslinked ion diffusion inhibitors stabilize 3D/2D perovskite heterostructures for efficient and stable photovoltaics

*Long Luo, Haipeng Zeng, Zaiwei Wang, Min Li, Shuai You, Bin Chen, Aidan Maxwell, Chao Wang, Shangzhi Li, Xueqing Cai, Weixi Li, Lin Li, Rui Guo, Rong Huang, Wenxi Liang, Yaoguang Rong*, Edward H. Sargent*, Xiong Li[1]**

[1]Michael Grätzel Center for Mesoscopic Solar Cells, Wuhan National Laboratory for Optoelectronics, Huazhong University of Science and Technology, Wuhan 430074, China

[2]Department of Electrical and Computer Engineering, University of Toronto, Toronto, Ontario, Canada

[3]State Key Laboratory of Advanced Technologies for Materials Synthesis and Processing, Wuhan University of Technology, Wuhan 430070, China

[4]Vacuum Interconnected Nanotech Workstation (Nano-X), Suzhou Institute of Nano-Tech and Nano-Bionics, the Chinese Academy of Sciences, Suzhou 215123, China

*Corresponding author. Email: ygrong@hust.edu.cn; ted.sargent@utoronto.ca; xiongli@hust.edu.cn

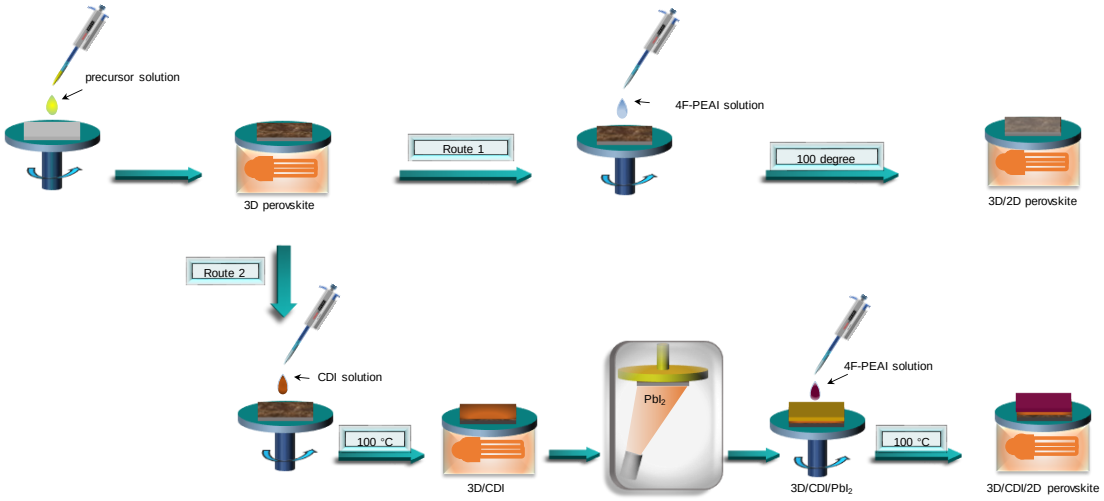


**Supplementary Figure 1 | Fabrication routes of perovskite heterostructures.** Route 1 is the traditional preparation process of a 3D/2D perovskite heterostructure by directly spin-coating 4F-PEAI/IPA solution on the 3D perovskite surface. Route 2 is the preparation process of a 3D/CDI/2D perovskite heterostructure where the 2D perovskite is prepared by a vapor-assisted two-step process.

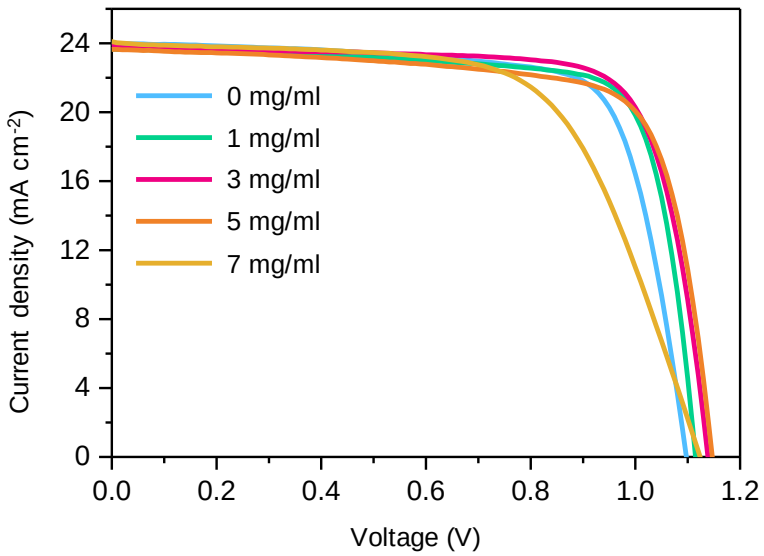


**Supplementary Figure 2 | J-V curves of 3D/CDI/2D devices with different concentrations of CDI precursor solutions.** The optimized concentration of CDI precursor solutions is 3 mg/ml.

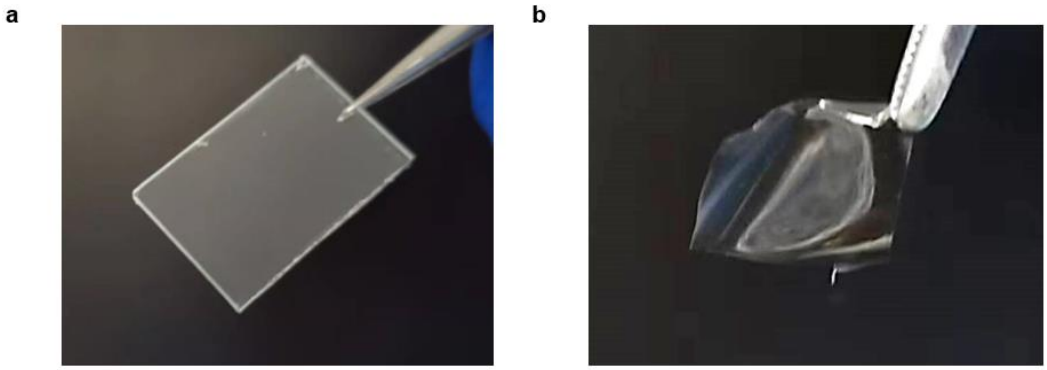


**Supplementary Figure 3 | Photo of a CDI film on a glass substrate. a,** The CDI thin film was deposited on the glass substrate by spin coating the CDI precursor solution (30 mg $mL^{-1}$ in tetrahydrofuran) at 200 rpm for 30 seconds. **b**, The CDI thin film was separated from glass substrate.

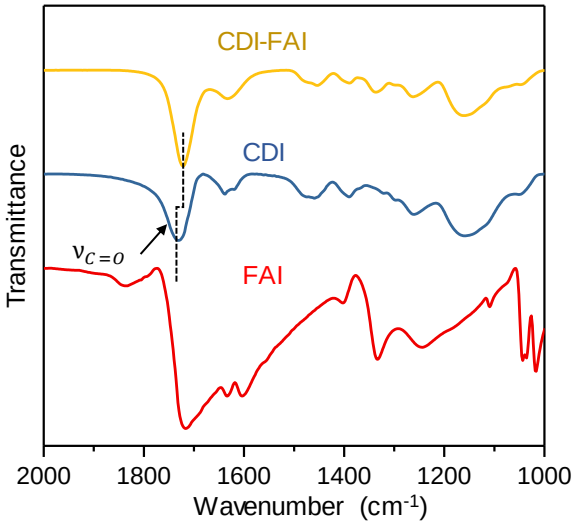


**Supplementary Figure 4 | FTIR spectra of FAI, CDI and CDI-FAI.**

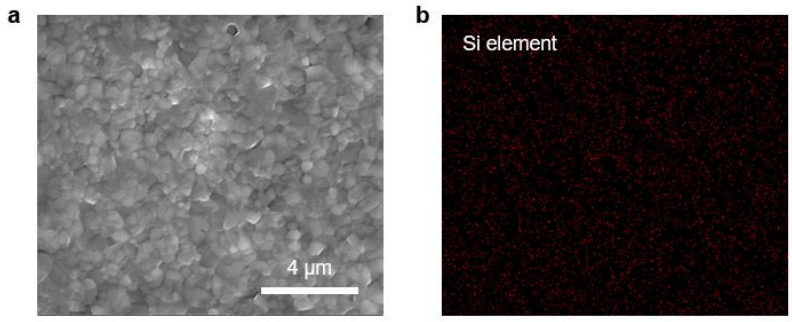


**Supplementary Figure 5 | Morphology and elemental distribution of a 3D perovskite/CDI film.** Surface SEM image (**a**) and the corresponding EDS (**b**) for a 3D perovskite/CDI film.

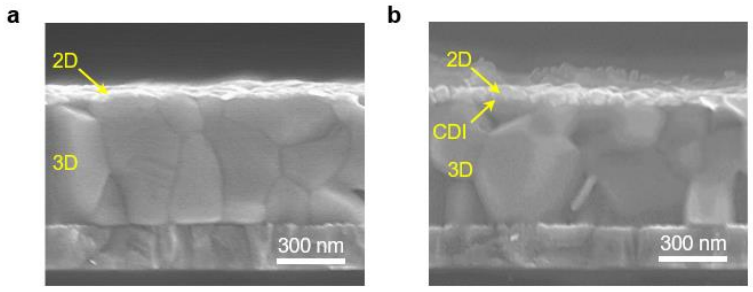


**Supplementary Figure 6 | The increased 2D thickness of 3D/CDI/2D perovskite heterostructures**. Cross-sectional SEM images of the 3D/2D (**a**) and 3D/CDI/2D (**b**) perovskite heterostructures.

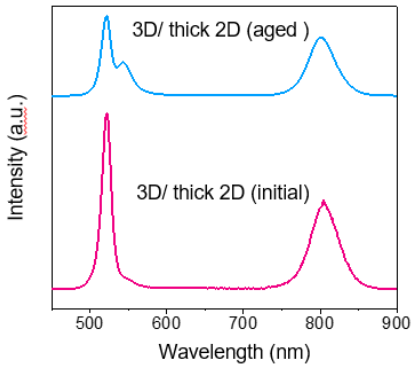


**Supplementary Figure 7 | Steady-state PL spectra measurement.** Steady-state PL spectra of initial and thermally-aged 3D/2D perovskite heterostructures with a thick 2D perovskite prepared by the same vapor-assisted two-step process as in the 3D/CDI/2D perovskite heterostructure.

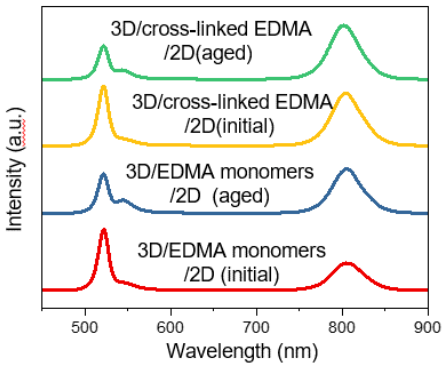


**Supplementary Figure 8 | Stability of 3D/2D perovskite heterostructures with different barrier layer.** Steady-state PL spectra of initial and thermally-aged 3D/2D perovskite heterostructures with EDMA monomer and crosslinked EDMA polymer as the barrier layer.

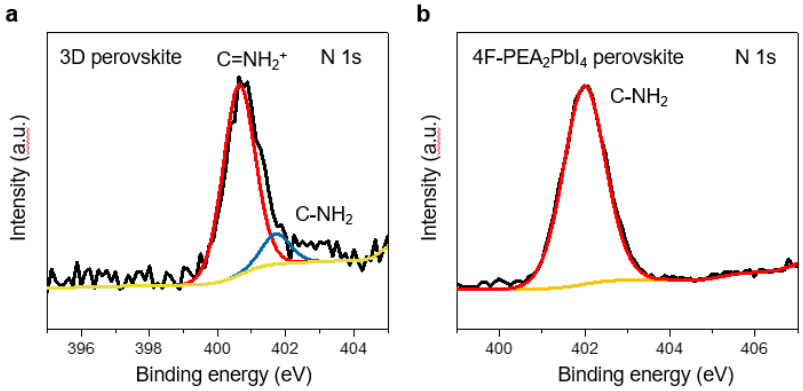


**Supplementary Figure 9 | XPS spectra measurement.** XPS spectra of 3D $(FAPbI_3)_{0.95}(MAPbBr_3)_{0.05}$ perovskite (**a**) and 2D 4F-$PEA_2PbI_4$ perovskite (**b**).

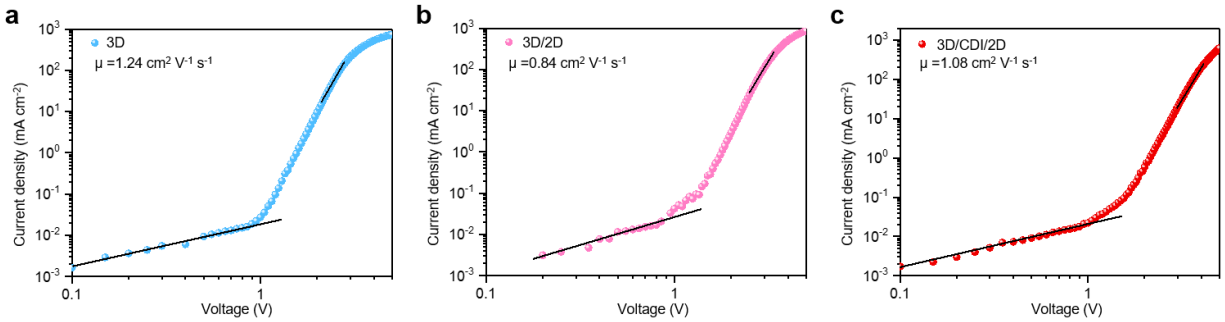


**Supplementary Figure 10 | Dark *J–V* characteristics of electron-only devices (ITO/$SnO_2$/perovskite heterostructure/PCBM/Au).**

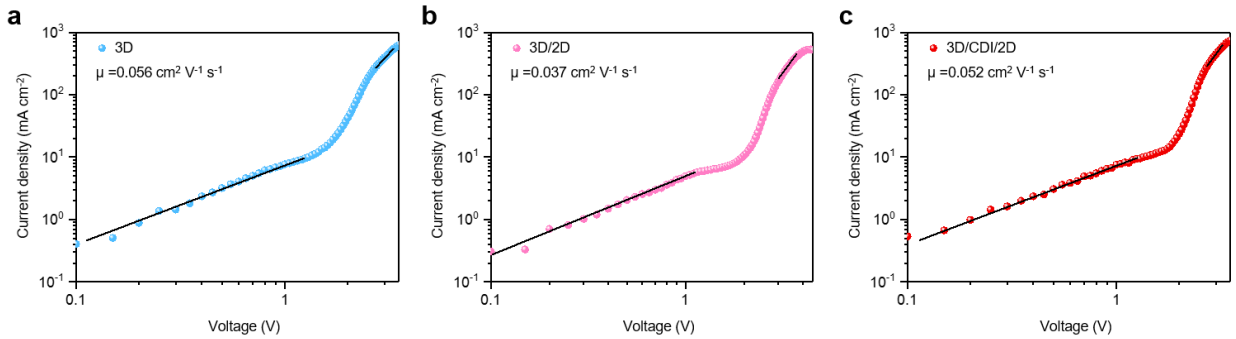


**Supplementary Figure 11 | Dark *J–V* characteristics of hole-only devices (ITO/PTAA/perovskite heterostructure /Spiro/Au).**

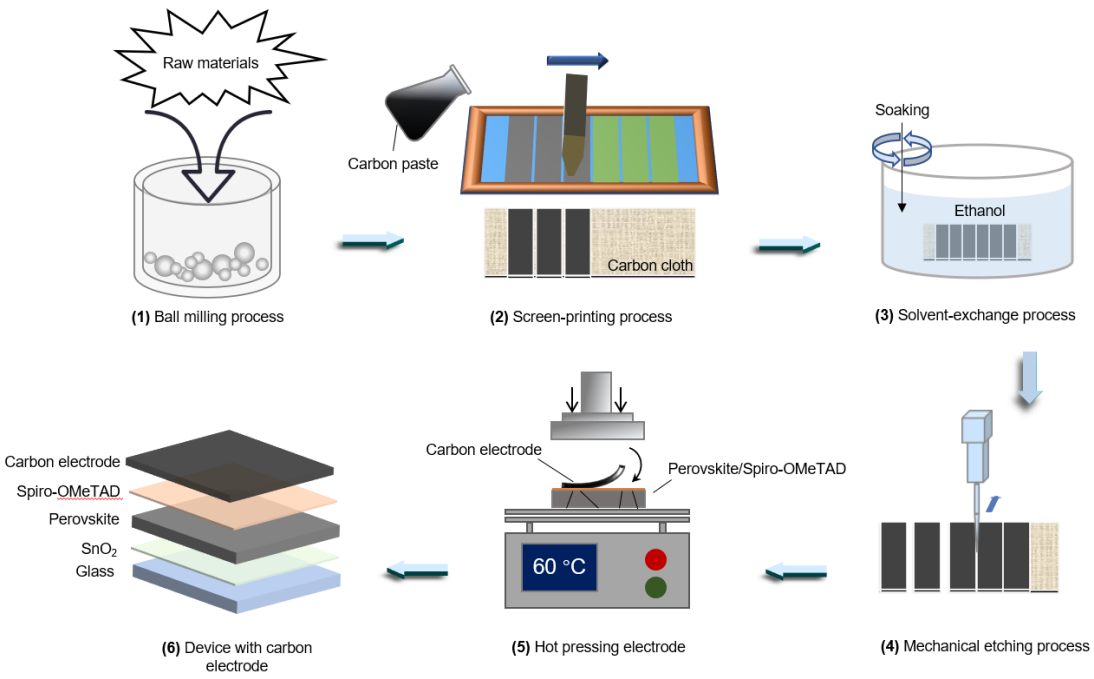


**Supplementary Figure 12 | Preparation process of carbon electrode based on the screen-printing technique.**

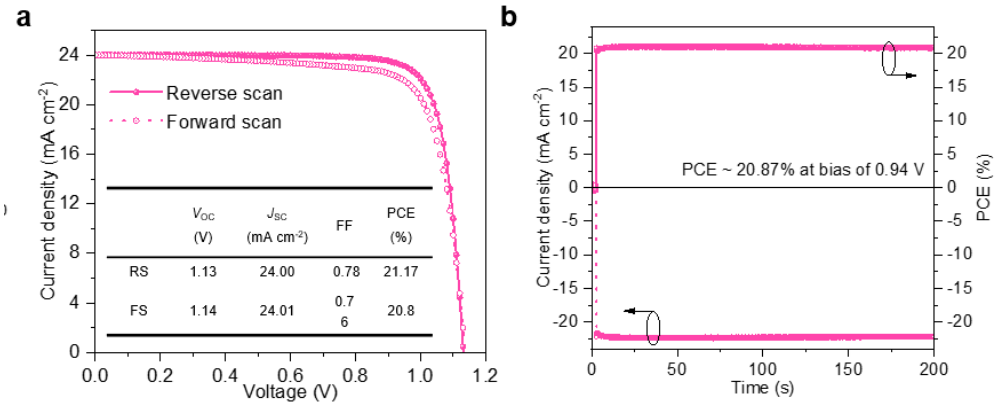


**Supplementary Figure 13 | Device performance of 3D/CDI/2D PSCs.** J-V curves (**a**) and the stabilized output and calculated PCE of the device at a fixed bias (**b**).

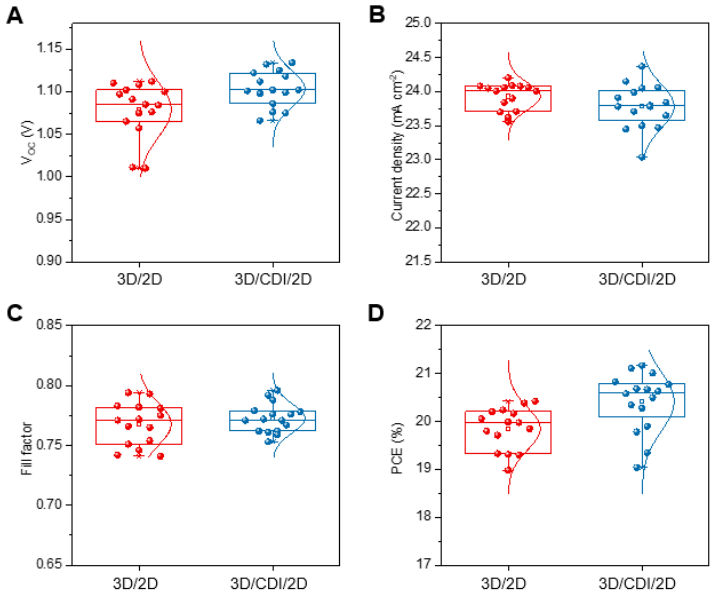


**Supplementary Figure 14 | The statistics of photoelectric performance parameters.** Comparison of the device performance obtained by 3D/2D and 3D/CDI/2D perovskite heterostructures.

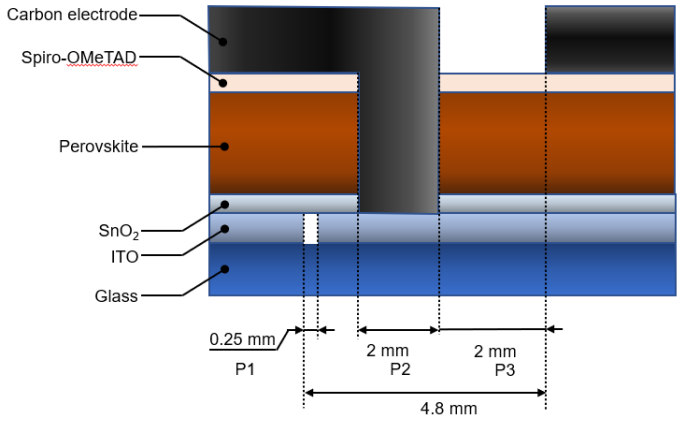


**Supplementary Figure 15 | Side view of the PSM.**

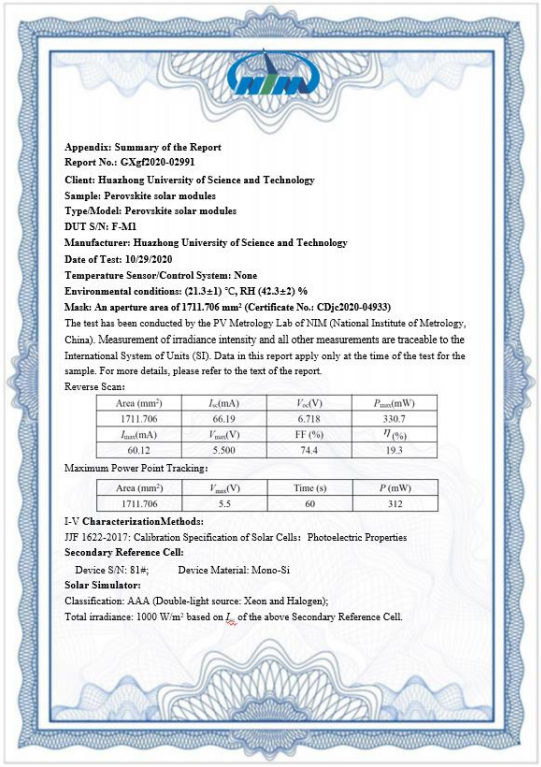

**Appendix: Summary of the Report**
**Report No.: GXgf2020-02991**
**Client: Huazhong University of Science and Technology**
**Sample: Perovskite solar modules**
**Type/Model: Perovskite solar modules**
**DUT S/N: F-M1**
**Manufacturer: Huazhong University of Science and Technology**
**Date of Test: 10/29/2020**
**Temperature Sensor/Control System: None**
**Environmental conditions: (21.3±1) °C, RH (42.3±2) %**
**Mask: An aperture area of 1711.706 mm² (Certificate No.: CDjc2020-04933)**
The test has been conducted by the PV Metrology Lab of NIM (National Institute of Metrology, China). Measurement of irradiance intensity and all other measurements are traceable to the International System of Units (SI). Data in this report apply only at the time of the test for the sample. For more details, please refer to the text of the report.
Reverse Scan:

| Area (mm²) | $I_{sc}$(mA) | $V_{oc}$(V) | $P_{max}$(mW) |
|---|---|---|---|
| 1711.706 | 66.19 | 6.718 | 330.7 |
| $I_{max}$(mA) | $V_{max}$(V) | FF (%) | $\eta$ (%) |
| 60.12 | 5.500 | 74.4 | 19.3 |

Maximum Power Point Tracking:

| Area (mm²) | $V_{max}$(V) | Time (s) | $P$ (mW) |
|---|---|---|---|
| 1711.706 | 5.5 | 60 | 312 |

I-V **CharacterizationMethods:**
IJF 1622-2017: Calibration Specification of Solar Cells: Photoelectric Properties
**Secondary Reference Cell:**
Device S/N: 81#; Device Material: Mono-Si
**Solar Simulator:**
Classification: AAA (Double-light source: Xeon and Halogen);
Total irradiance: 1000 W/m² based on $I_{sc}$ of the above Secondary Reference Cell.

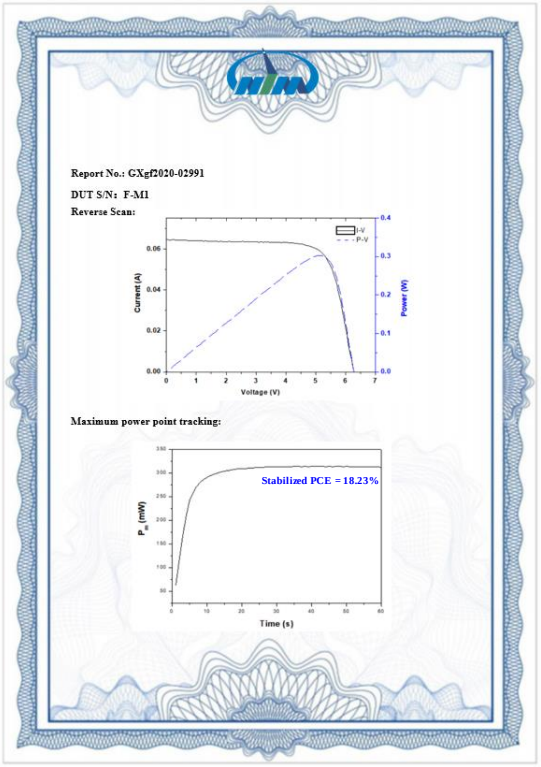


**Supplementary Figure 16 | Certification of a PSM based on the 3D/CDI/2D perovskite heterostructure and carbon electrode.** The aperture area is 17.12 $cm^2$, and the stabilized PCE is 18.23%. Certification was carried out by the National Institute of Metrology in China.

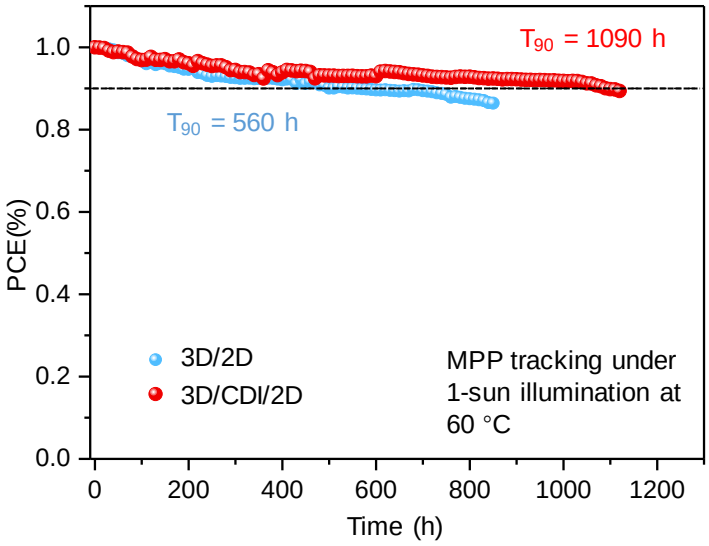


**Supplementary Figure 17 | The operational stability of PSCs ($SnO_2$/perovskite heterostructure/Spiro-OMeTAD/Carbon) under continuous illumination in $N_2$ at ~60 °C.** For the 3D/2D device, the initial efficiency is 20.15%. For the 3D/CDI/2D device, the initial efficiency is 21.02%.

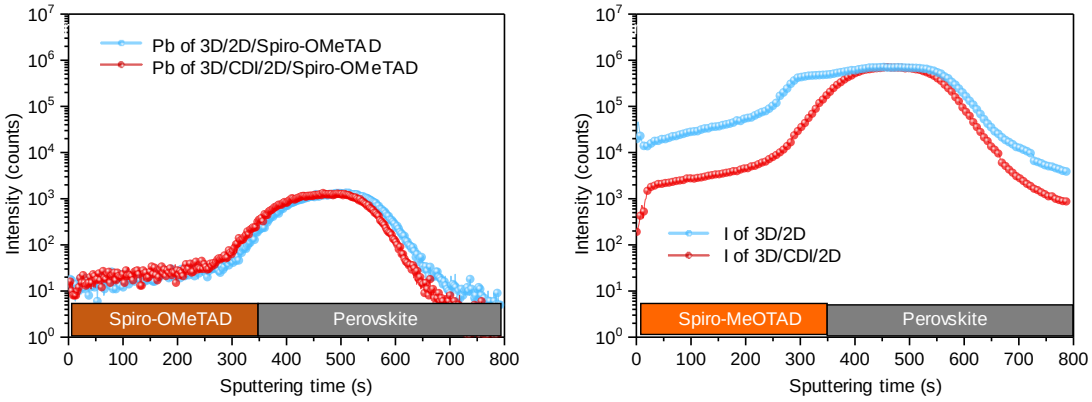


**Supplementary Figure 18 | TOF-SIMS of Pb and I ions in Spiro-OMeTAD and the perovskite layer.**

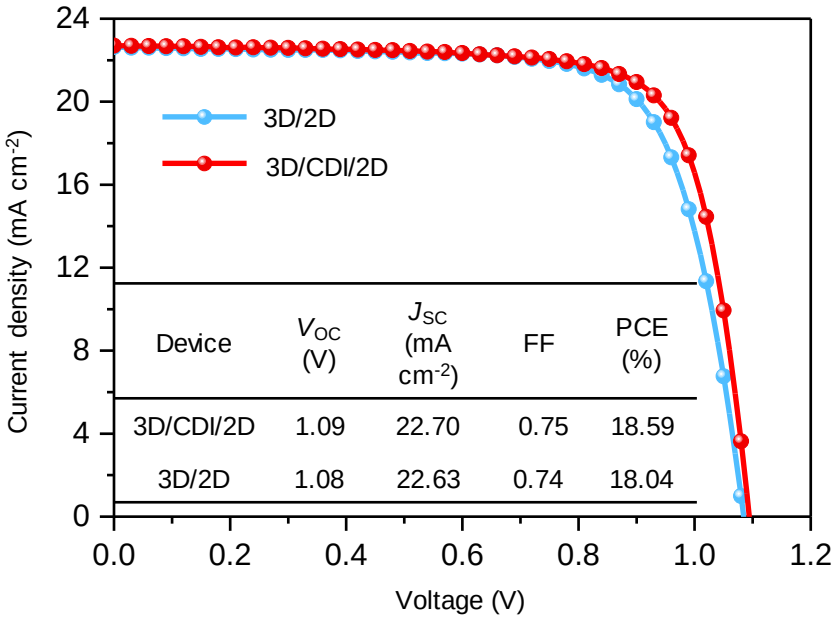


**Supplementary Figure 19 | Device performance obtained with P3HT-Spiro-OMeTAD.** The *J-V* curves of PSCs with the structure of $SnO_2$/ (3D/2D perovskite)/P3HT-Spiro-OMeTAD/Carbon, and $SnO_2$/ (3D/CDI/2D perovskite)/P3HT-Spiro-OMeTAD/Carbon.

**Supplementary Table 1 |. Summary of reported operating stability of PSCs.** The perovskite layer is treated with bulky organics, and the back contact is either metal (Au, Ag and Cu) or carbon. (Ref [1-19]).

| Perovskite passivation | Electrode | PCE/% (Aperture area/cm$^2$) | Lifetime （MPP） | T (°C) | Journal/Year |
|---|---|---|---|---|---|
| **CDI/4F-PEAI** | **Carbon** | **21.17 (0.16)** | **$T_{90}$ = 4392 hrs** | **60 °C** | **This work** |
| **CDI/4F-PEAI** | **Carbon** | **18.2 (17.1)** | - | - | **This work-** |
| MeO-PEAI (ST) | Au | 25.8 (0.096) | $T_{90}$ = ~ 500 hrs | - | *Nature* (2021, Ref. 1) |
| FAHCOO (BT) /OAI (ST) | Au | 25.6 (0.08) | $T_{85}$ = 450 hrs | 35 | *Nature* (2021, Ref. 2) |
| $DMePDAI_2$ (ST) | Au | 24.7 (0.12) | $T_{90}$ = 1000 hrs | ~ 40 | *Science* (2021, Ref. 3) |
| OLAI (ST) | Ag | 24.3 (0.07) | $T_{95}$ = 500 hrs | ~ 40 | *Science* (2022, Ref. 4) |
| 3F-PEAI/MAI (ST) | Ag | 23.3 (0.05) | No degradation = 1000 hrs | RT | *Nat. Photon.* (2022, Ref. 5) |
| 3F-PEAI/MAI (ST) | Ag | 23.3 (0.05) | $T_{92}$ = 500 hrs | 65 | *Nat. Photon.* (2022, Ref. 5) |
| choline chloride (ST) | Au | 23.1 (0.16) | $T_{90}$ = 500 hrs | RT | *Science* (2020, Ref. 6) |
| i-BABr (ST) | Au | 20.42 (17.1) | $T_{82}$ = 500 hrs | RT | *Science* (2021, Ref. 7) |
| $BA_2PbI_4$ (ST) | Au | 24.35 (0.094) | $T_{98}$ = 1620 hrs | - | *Nat. Energy* (2021, Ref. 8) |
| EAI/MAI (ST) | Au | 16.6 (22.4) | $T_{90}$ = 1570 hrs | 40 | *Nat. Energy* (2020, Ref. 9) |
| OATsO (ST) | Au | 24 (0.13) | No degradation = 800 hrs | 40 | *Nature* (2022, Ref. 10) |
| iPAmHCl (BT) | Au | 23.9 (0.16) | No degradation, 2000 hrs | RT | *Nat. Energy* (2021, Ref. 11) |
| - | Au | 24.04 (0.08) | $T_{95}$ = ~ 2000 hrs | RT | *Science* (2021, Ref. 12) |
| - | rGO/ Au | 20.4 (0.16) | $T_{95}$ = 1000 hrs | 60 | *Science* (2019, Ref. 13) |
| - | Ag | 22.02 (0.13) | $T_{92}$ = 1000 hrs | 85 | *Nat. Nanotechnol.* (2020, Ref. 14) |
| $PbPyA_2$/TMS (ST) | Cu | 24.3 (0.09) | $T_{90}$ = 1000 hrs | 55 | *Science* (2022, Ref. 15) |
| lead sulfate (ST) | Cu | 21.1 (-) | $T_{97}$ = 1200 hrs | 65 | *Science* (2019, Ref. 16) |
| - | Cu | 20.1 (17.9) | No degradation = 550 hrs | 60 | *Science* (2021, Ref. 17) |
| - | $Ti_1$-rGO/FTO | 20.6 (0.09) | $T_{95}$ = 1300 hrs | 60 | *Nat. energy* (2021, Ref. 18) |
| - | Au/$MgF_2$ | 20.9 (0.113) | No degradation, 1400 hrs | 60~65 | *Nat. Energy* (2021, Ref. 19) |

Note:
4-methoxy-phenethylammonium iodide: MeO-PEAI; octylammonium iodide: OAI; Octylammonium tosylate: OATsO; N, N-dimethyl-1,3-propane diammonium diiodide: $DMePDAI_2$; Oleylammonium iodide: OLAI; isobutylamine bromide: i-BABr. 3-iodopropyl trimethoxysilane [Si $(OCH_3)_3(CH_2)3_I$]: I-SAM; Polyethylenimine: PEIE; poly[2,2‴-bis[[(2-butyloctyl)oxy]carbonyl] [2,2′:5′,2″:5″,2‴-quaterthiophene]-5,5‴-diyl]): PDCBT; BCF-doped poly(triarylamine): PTAA-BCF; 4-fluoro-phenethylammonium iodide: 4F-PEAI; 3-fluoro-phenethylammonium: 3F-PEAI; pyrene-based ethylammonium iodide: PREAI; isopropylammonium chloride: iPAmHCl; n-hexyl trimethyl ammonium bromide: HTABr; ethylenediaminetetraacetic acid dipotassium salt: EDTAK;

ethylammonium iodide: EAI; aminovaleric acid iodide: AVAI; 5-ammoniumvaleric acid iodide: 5-AVAI; 1-butyl-3-methylimidazolium tetrafluoroborate: BMIMBF4; Pyridine-2-carboxylic lead: PbPyA2; Hexamethyldisilathiane: TMS; Maximum power point tracking: MPPT; Surface treatment: ST; Bulk treatment: BT; Room temperature: RT.

**Supplementary Table 2 | The fitted parameters from TRPL of various perovskite samples.**

| Samples | $A_1$ | $\tau_1$ | $A_2$ | $\tau_2$ | $\tau_{avg}$ (ns) |
|---|---|---|---|---|---|
| Pristine 3D | 0.569 | 91.3 | 0.431 | 455.42 | 248.24 |
| 3D/2D | 0.527 | 83.72 | 0.473 | 573.65 | 315.46 |
| 3D/CDI/2D | 0.491 | 89.17 | 0.509 | 824.72 | 423.56 |
| Pristine 3D/ Spiro-OMeTAD | 0.645 | 5.62 | 0.355 | 55.02 | 23.16 |
| 3D/2D/Spiro-OMeTAD | 0.639 | 7.71 | 0.361 | 68.15 | 29.53 |
| 3D/CDI/2D /Spiro-OMeTAD | 0.641 | 6.73 | 0.359 | 62.1 | 26.61 |

**Note:** The measured PL decay kinetics are fitted by bi-exponential decay function as follow

$F(t) = A_1 \exp(-t/\tau_1) + A_2 \exp(-t/\tau_2)$

The average lifetime: $\tau_{avg} = (A_1 * \tau_1 + A_2 * \tau_2)/(A_1 + A_2)$

## Supplementary References


1. Min, H. *et al.* Perovskite solar cells with atomically coherent interlayers on SnO2 electrodes. *Nature*, **598**, 444-450 (2021).
2. Jeong, J. *et al.* Pseudo-halide anion engineering for α-FAPbI3 perovskite solar cells. *Nature*, **592**, 381-385 (2021).
3. Zhang, F. *et al.* Metastable Dion-Jacobson 2D structure enables efficientand stable perovskite solar cells. *Science*, **375**, 71-76 (2021).
4. Azmi, R. *et al.* Damp heat–stable perovskite solar cells with tailored-dimensionality 2D/3D heterojunctions. *Science*, **376**, 73-77 (2022).
5. Chen, H. *et al.* Quantum-size-tuned heterostructures enable efficient and stable inverted perovskite solar cells. *Nat. Photon.*, **16**, 352-358 (2022).
6. Lu, H. *et al.* Vapor-assisted deposition of highly efficient, stable black-phase FAPbI3 perovskite solar cells. *Science*, **370**, abb8985 (2020).
7. Bu, T. *et al.* Lead halide–templated crystallization of methylamine-free perovskite for efficient photovoltaic modules. *Science*, **372**, 1327-1332 (2021).
8. Jang, Y.-W. *et al.* Intact 2D/3D halide junction perovskite solar cells via solid-phase in-plane growth. *Nat. Energy*, **6**, 63-71 (2021).
9. Liu, Z. *et al.* A holistic approach to interface stabilization for efficient perovskite solar modules with over 2,000-hour operational stability. *Nat. Energy*, **5**, 596-604 (2020).
10. Tan, S. *et al.* Stability-limiting heterointerfaces of perovskite photovoltaics. *Nature*, **605**, 268-273 (2022).
11. Park, B.-W. *et al.* Stabilization of formamidinium lead triiodide α-phase with isopropylammonium chloride for perovskite solar cells. *Nat. Energy*, **6**, 419-428 (2021).
12. Li, N. *et al.* Liquid medium annealing for fabricating durable perovskite solar cells with improved reproducibility. *Science*, **373**, 561-567 (2021).
13. Arora, N. *et al.* Perovskite solar cells with CuSCN hole extraction layers yield stabilized efficiencies greater than 20%. *Science*, **358**, 768-771 (2017).
14. Wu, S. *et al.* 2D metal–organic framework for stable perovskite solar cells with minimized lead leakage. *Nat. Nanotechnol.*, **15**, 934-940 (2020).
15. Li, X. *et al.* Constructing heterojunctions by surface sulfidation for efficient inverted perovskite solar cells. *Science*, **375**, 434-437 (2022).
16. Yang, S. *et al.* Stabilizing halide perovskite surfaces for solar cell operation with wide-bandgap lead oxysalts. *Science*, **365**, 473-478 (2019).
17. Chen, S. *et al.* Stabilizing perovskite-substrate interfaces for high-performance perovskite modules. *Science*, **373**, 902-907 (2021).
18. Zhang, C. *et al.* Ti1–graphene single-atom material for improved energy level alignment in perovskite solar cells. *Nat. Energy*, **6**, 1154-1163 (2021).
19. Zhao, Y. *et al.* A bilayer conducting polymer structure for planar perovskite solar cells with over 1,400 hours operational stability at elevated temperatures. *Nat. Energy*, **7**, 144-152 (2021).